Journal of Optimization in Industrial Engineering
Vol.15, Issue 2, Summer & Autumn 2022, 45- 55
Doi: 10.22094/joie.2022.1943281.1906

Research Article

A New Fuzzy controller for Damping of Sub Synchronous Resonance (SSR) in the modified IEEE First Bench Mark

Yaser Bostani [a] , Saeid Jalilzadeh[a,*]

[a] *Department of Electrical Engineering, University of Zanjan, Zanjan, Iran*

Received 24 October 2021; Revised 01 February 2022; Accepted 06 February 2022

Abstract
In this paper, the mitigating subsynchronous resonance (SSR) phenomenon has been designed in modified IEEE- first bench mark including DFIG-based wind farms connected compensated transmission lines that includes a series capacitor with fuzzy controller. In addition, wide- area measurement systems have been used in the fuzzy controller. This paper designs a fuzzy logic wide-area damping controller to mitigate SSR by considering the time delay caused by the (Phasor Measurement Unit) PMU measurement. The fuzzy controller is a supplementary signal at the stator voltage of the gird-side converter (GSC) of DFIG-primarily based wind farms. This controller is executed by including voltage and capacitor voltage variations of series capacitive compensated. The effectiveness and validity of the proposed auxiliary damping control had been verified on a modified scheme of the IEEE- first benchmark model via time area simulation analysis by using MATLAB/Simulink.

Keywords: Fuzzy controller; Double fed induction generator; Rotor-side convertor; Grid-side convertorSC; Subsynchronous resonance

Nomenclature

SSR	Sub-synchronous resonance
wams	Wide area measurement system
pmu	Phasor measurement unit
IGE	Inductive generating effects
DFIG	Doubly fed induction generator
TI	Torsional interference
IGE	Induction generator effect
GSC	Gird side convertor
RSC	Rotor side convertor
Wb	Synchronous Speed
Twind	Wind torque
Wt	Wind turbine Speed
Pr	Active power of the RSC converter
Pg	Active power of the GSC converter.
Rs	Stature resistance
Rr	Rotor resistance
Te	Electric torque of the generator
i_{qs}	Stator's currents in the qd0-frame
i_{ds}	Stator's currents in the qd0-frame
i_{qr}	Rotor's currents in the qd0-frame
i_{dr}	Rotor's currents in the qd0-frame
V_{qs}	Stator's voltages in the qd0-frame
V_{ds}	Stator's voltages in the qd0-frame
V_{qr}	Rotor's voltages in the qd0-frame
V_{dr}	Rotor's voltages in the qd0-frame
X_M	Magnetic reactance
X_{lr}	Rotor leakage reactance
X_{ls}	Stator leakage reactance
ω_b	Synchronous frequency
ω_r	Rotor frequency
ω	Base frequency
fs	Synchronous frequency
fn	Natural frequency
fr	Rotor electrical frequency

1. Introduction

Due to the restructuring of power systems, system features have changed somewhat, including the transmission system, and have exceeded their stable range. T he problems in the construction of power transmission lines have forced the generating institutions to obtain maximum efficiency from energy transmission lines by methods such as compensation (Piwko, 2006). One method is to compensate the series

*Corresponding author Email address: jalilzadeh@znu.ac.ir

capacitor. The application of the series capacitor causes an increase in power transmission capacity of the lines and improvement of system stability. Despite all of the advantages it has, the series capacitor causes fluctuations with frequencies less than the nominal frequency of the network, known as SSR (Fan L. Z., 2011). In addition, using wind energy has developed. The power of wind farms based on a doubly fed induction generator (DFIG) has been installed worldwide. If the DFIG-based wind farm becomes with the capacitive series compensated transmission lines, the possibility of latest the subsynchronous resonance (SSR) phenomenon occurring will grow in power systems (Mohammadpour, 2015). The SSR phenomenon is divided into induction generator effect (IGE), and torsional interaction (TI) in wind farms interfaced with series compensated transmission lines. In reality, the SSR phenomenon in induction machines is IGE, due to wind generators, the frequency torsional modes can be as little as 1-3 Hz. On the other hand, torsional interaction mode must have a frequency of fifty-seven to fifty-nine Hz (Tapia, 2003) . So far, many studies have been conducted in the field of SSR. Some focused on the damped oscillation of SSR using an additional controller in RSC, and GSC of DFIG based wind farm converters, while some emphasized damped SSR using FACTS devices replaced with a series capacitor and applied control to these devices. The following, some of which will be reviewed here. The rotor velocity has been used in SSR mitigation control (Piwko, 2006). With using recording tools in series compensataion transmission line has linked with wind electricity. Varma et al. explored TCSC and SVC's capability in SSR mitigation at the same time as in , STATCOM's capability in SSR mitigation has been explored. The state wind energy structures use DFIGs with back-to-returned power electronic converters (Suriyaarachchi, 2012,july). The capability of modern-day such as converters in the most energy point tracking and voltage/reactive power control (Mohammadpour, 2015), compensation for unbalanced grid situations (Sahni, 2012, July), and oscillation stability (Fan, 2010), (Wang, 2013) have been explored in the literature. However, the manipulated potential of these converters in mitigating SSR has not yet been investigated now (Hughes, 2006). Reference (Wang, 2013) investigates SSR in series compensated fixed speed wind generation systems that employ self-excited double cage induction generators. PSCAD simulations are conducted to demonstrate IGE and TI. The paper concludes that the greater the output power from wind farms, the lesser the system damping. However, variable speed wind generation systems employing DFIG offer greater operational flexibility and improved efficiencies and hence, are rapidly gaining ground as opposed to fixed speed systems.

Reference (Xie, 2014, October) presents purely time-domain simulations without small-signal (eigenvalue) analysis, which is required to understand the damping of modal oscillations related to SSR. In (El-Moursi, 2009) presents the modeling and stability of a DFIG-based wind farm interfaced with series compensation. The impact of parameters such as wind speed, compensation level, and current controller parameters on system damping under subsynchronous frequency are studied. However, (Tapia, 2003) does not differentiate the two SSR phenomena and does not present the relationship of turbine parameters and torsional oscillation modes. Thus, the focus of this paper is to systematically examine SSR in DFIG-based series compensated systems. While a preliminary analysis appears in (Tapia, 2003), a detailed analysis has been carried out in this paper to identify under what parametric conditions the IGE and TI The system models in this paper are developed in MATLAB/Simulink for the ease of small-signal analysis as well as time-domain simulations. However, other tools such as PSCAD/EMTDC (Xu L. &., 2007) or ATP/EMTP (Hughes F. M.-L., 2006) have also been used for time-domain SSR simulations. In (Raju, 2016), the IEEE first benchmark model is adopted for this study, and the superiority of the FOPI based UPFC controller over PI-based UPFC controller is discussed by comparing the results with various performance indices. In (Dhenuvakonda, 2018), it proposes a powerful fractional-order PI controller to mitigate the subsynchronous oscillations in the turbine-generator shaft due to subsynchronous resonance (SSR) with FACTS devices. In (Vajpayee, 2020, July), it explores a robust Fractional-order PI (FOPI) controller to diminish subsynchronous resonance (SSR) using a static synchronous series compensator (SSSC). The insertion and fine-tuning of the fractional-order PI controller in the control scheme of SSSC the subsynchronous oscillations are reduced to 4 % as compared to the conventional PI controller. In (Dametew, 2021), a new approach is proposed for mitigating the problems associated with distance protection by using the synchrophasor measurement. The entire study of simulation is investigated by using a 48-pulse SSSC carried out with the Bergeron model of transmission line in PSCAD. However, WAMS is widely used in power systems in recent years. The use of WAMS is justified since the DFIG based wind farm is usually offshore and far from the compensated power system and transmission lines (Mohammadpour, Modeling and control of gate-controlled series capacitor interfaced with a DFIG-based wind farm., 2014), which is important since the additional controller is for SSR attenuation in DFIG controllers, and this study used voltage and compensator capacitor voltage variations for additional controller inputs. In fact, the measurement of input quantities in WAMS is done by using phasor measurements units (PMU), which is one of the main components of WAMS. However, the delay of measurement signals by the PMU should be considered in designing the controller. The controller may even cause instability while ignoring the latency (Mohammadpour H. A., 2014, March).

In this studies, fuzzy controller was proposed to reduce the impact of subsynchronous resonance for DFIG-based wind farms by considering time latencies in communication networks. In this regard, WAFC was designed based on the Mamdani inference structures in which voltage and compensator capacitor voltage variations are considered as inputs for additional controller to the controller, and GSC brand

DFIG is the new output.
The remainder of this paper is as follows. Section 2 describes the studied modeling system. Section 3 offers the background for the SSR phenomenon in fixed series compensated DFIG, and the eigenvalues are obtained. Section 4 describes the design wide- area fuzzy logic controller (FLWADC) based on the Mamdani inference system. Section 5 discusses the case study and time domain simulation end result. Finally, the conclusions are made in Section 6.

2. Modeling of the Studied System

A wind power plant with DFIG is used to analyze the dynamic stability and SSR phenomenon, which is connected to an infinite bus with a compensated transmission line of capacitive series which is the modified IEEE as the first benchmark (Figure 1).

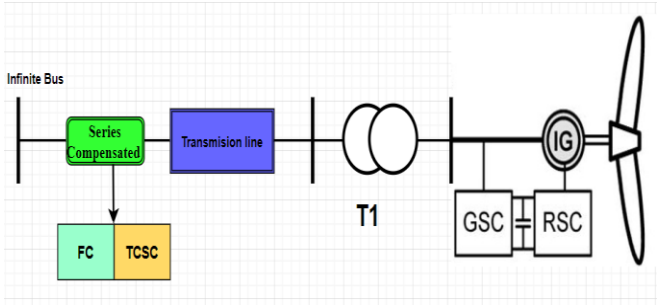

Fig.1. Single Line Diagram of the studied system

According to the references (Tapia, 2003) (Bialasiewicz, 2006, November)a wind farm can be modeled as an equivalent wind farm because all the parameters of a wind farm are similar to an equivalent wind farm. In this regard, only the power of the wind farm is equal to the DFIGs' total power. For example, a wind farm with fifty 2 MW generators, is modeled as a 100 MW generator (El-Moursi, 2009). The parameters of a 2-MW DFIG and the aggregated DFIG are shown in appendix.

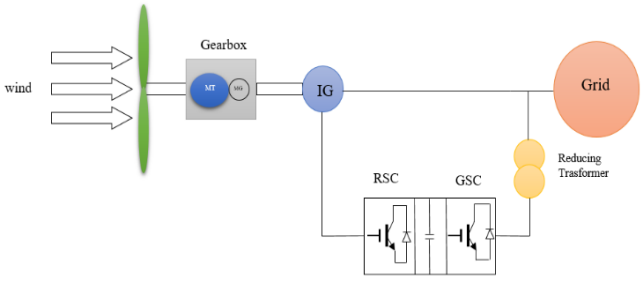

Fig. 2. Single Line model of DFIG

2.1. Equations of induction generator in dq0 frame

Induction generator in dq0 reference frame is in the form of modeling equations (1-3) (Xu L. &., 2007) :

$$\dot{X} = AX + BU \quad (1)$$

$$X = [i_{qs} \,.\, i_{ds} \,.\, i_{qr} \,.\, i_{dr}]^T \quad (2)$$

$$U = [V_{qs} \,.V_{ds} \,.\, V_{qr} \,.\, V_{dr}]^T \quad (3)$$

$$\frac{d}{dt}\begin{bmatrix} i_{qs} \\ i_{ds} \\ i_{os} \\ i_{qr} \\ i_{dr} \\ i_{or} \end{bmatrix} = A\begin{bmatrix} i_{qs} \\ i_{ds} \\ i_{os} \\ i_{qr} \\ i_{dr} \\ i_{or} \end{bmatrix} + B\begin{bmatrix} V_{qs} \\ V_{ds} \\ V_{os} \\ V_{qr} \\ V_{dr} \\ V_{or} \end{bmatrix} \quad (4)$$

$$A = -\omega_b G^{-1} F \quad (5)$$

$$B = \omega_b G^{-1} \quad (6)$$

$$G = \begin{bmatrix} X_{ss} & 0 & 0 & X_M & 0 & 0 \\ 0 & X_{ss} & 0 & 0 & X_M & 0 \\ 0 & 0 & X_{ls} & 0 & 0 & 0 \\ X_M & 0 & 0 & X_{rr} & 0 & 0 \\ 0 & X_M & 0 & 0 & X_{rr} & 0 \\ 0 & 0 & 0 & 0 & 0 & X_{lr} \end{bmatrix} \quad (7)$$

$$F = \begin{bmatrix} R_s & \frac{\omega}{\omega_b}X_{ss} & 0 & 0 & \frac{\omega}{\omega_b}X_M & \\ -\frac{\omega}{\omega_b}X_M & R_s & 0 & -\frac{\omega}{\omega_b}X_M & 0 & \\ 0 & 0 & R_s & 0 & 0 & \\ 0 & \frac{(\omega-\omega_r)}{\omega_b}X_M & 0 & R_r & \frac{(\omega-\omega_r)}{\omega_b}X_{rr} & \\ -\frac{(\omega-\omega_r)}{\omega_b}X_{rr} & 0 & 0 & -\frac{(\omega-\omega_r)}{\omega_b}X_M & R_r & \end{bmatrix} \quad (8)$$

The state-space matrix of the induction generator relation can be expressed as (4) that, shows variables, which are the same as the stator and rotor currents at the two axes d and q. The items of Equation (4) are defined by (5) and (6). Also, G and F of equations (5) and (6) are defined by (7) and (8).
Where $\boldsymbol{\omega_b}$ shows synchronous frequency that is value is equal to 314 radians per second, w is the Angular Frequency of the rotating frame as dq0, R_s indicates stator resistance, and Rr is considered as the resistance of the rotor. In addition, Xm, Xls, Xlr, X_{ss} , and X_{rr} indicate magnetic reactance, stator leakage reactance, rotor leakage reactance , total stator reactance, and total rotor reactance, respectively. All of the values are in terms of the per-unit system (PU).

2.2. Modeling wind turbine shaft

In the SSR study, the turbine shaft model is equivalent to two masses, which reduces the volume of calculations in addition to sufficient accuracy. In this model, the low-speed mass is connected to the wind turbine shaft and the high-speed mass is connected to the generator rotor shaft (Hughes, 2006).

$$\frac{d}{dt}\begin{bmatrix} \omega_t \\ \omega_r \\ T_{tg} \end{bmatrix} = \begin{bmatrix} \frac{(-D_t - D_{tg})}{2H_t} & \frac{D_{tg}}{2H_t} & -\frac{1}{2H_g} \\ \frac{D_{tg}}{2H_g} & \frac{(-D_t - D_{tg})}{2H_t} & \frac{1}{2H_g} \\ K_{tg}.\,\omega_b & -K_{tg}.\,\omega_b & 0 \end{bmatrix} \times \begin{bmatrix} \omega_t \\ \omega_r \\ T_{tg} \end{bmatrix} + \begin{bmatrix} \frac{T_{wind}}{2H_t} \\ \frac{T_e}{2H_g} \\ 0 \end{bmatrix} \quad (9)$$

Where Wt represents the speed of wind turbine, Wr indicates the speed of the generator rotor, and Ttg stands for torsional torque or internal torque between two objects. Twind is considered as the torque generated by the wind and Te is the electric torque of the generator. All variables in relations are in unit value (Per-unit). The wind turbine electrical torque is calculated from Equation (10). The reference electrical torque is determined to obtain the maximum PowerPoint (MPPT), as shown in Table 1. The amounts of rotor speed, turbine power, and electric torque are calculated at each wind speed.

$$T_e = 0.5X_m(i_{qs}i_{dr} - i_{ds}i_{qr}) \quad (10)$$

Table 1
MPPT Lookup table

Vw(m/s)	7	8	9	10	11	12
ωr(pu)	0.75	0.85	0.95	1.05	1.15	1.25
Pwind(pu)	0.32	0.49	0.69	0.95	1.25	1.6
Twind=Pwind/ ωr	0.43	0.58	0.73	0.90	1.09	1.28

2.3. Model of DFIG converter controllers

DFIG converters require dynamic modeling (Fig. 2). To dynamically model and study the SSR phenomenon, the controllers are used to controll the RSC and GSC converters (Figure.3). In addition, MPPT is applied for the RSC controller with the help of the Lookup table and is considered in the turbine shaft model for wind torque (Twinds).

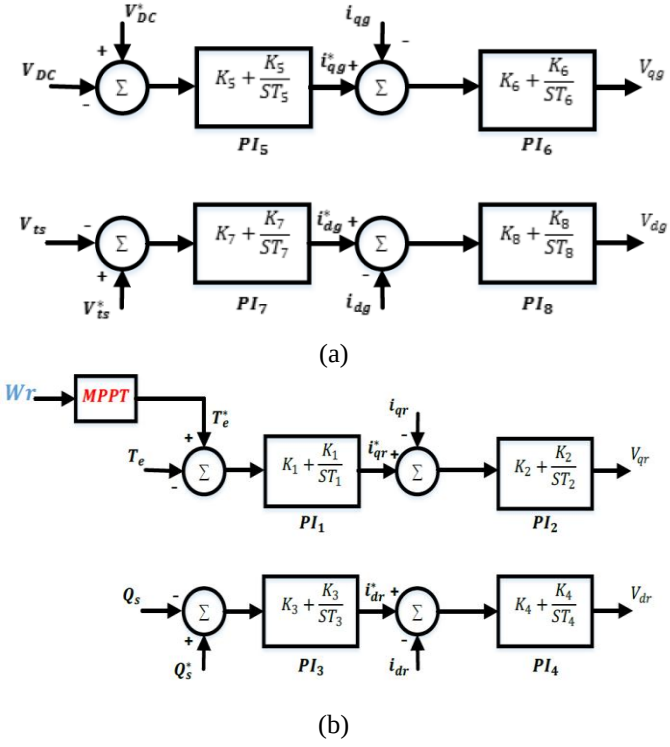

(a)

(b)

Fig. 3. GSC Controller (a) and RSC Controller (b) wind turbine with DFIG

2.4. Model of DC link Capacitor DFIG converter controllers

The DC loop capacitor dynamic between DFIG converters are modeled as first-order relationships as shown in Equations (11-13). Furthermore, ir and ig are the output currents of two converters, RSC and GSC, respectively. Figure. 4 shows how power is distributed in the DC loop between RSC and GSC converters.

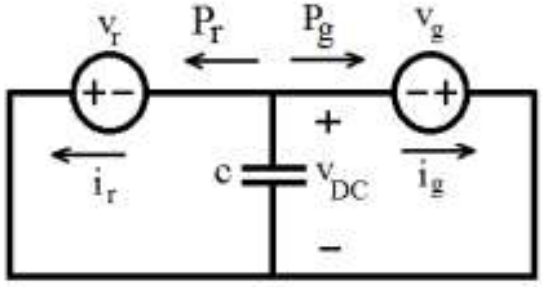

Fig. 4. DC link Capacitor of DFIG

$$cV_{DC}\frac{dV_{DC}}{dt} = -(P_r + P_g) \quad (11)$$

$$P_r = 0.5(V_{qr}i_{qr} + V_{dr}i_{dr}) \quad (12)$$

$$P_g = 0.5(V_{qg}i_{qg} + V_{dg}i_{dg}) \quad (13)$$

Where Pr shows the true power of the RSC converter, and Pg indicates the active power of the GSC. Vr and VG are the output voltages of the two converters RSC and GSC, respectively.

2.5- Differential equations of the capacitive series-compensated line

In this study, the transition with a grade 4 of the model of differential equations is expressed as equation 14 (Hughes F. M.-L., 2006):

$$\begin{bmatrix} \dot{I}_{qL} \\ \dot{I}_{dL} \\ \dot{V}_{qc} \\ \dot{V}_{dc} \end{bmatrix} = \begin{bmatrix} \frac{-R_L}{X_L}\omega_b & -\omega & -\frac{1}{X_L}\omega_b & 0 \\ \omega & \frac{-R_L}{X_L}\omega_b & 0 & -\frac{1}{X_L}\omega_b \\ \omega_b X_c & 0 & 0 & -\omega \\ 0 & \omega_b X_c & \omega & 0 \end{bmatrix} \begin{bmatrix} I_{qL} \\ I_{dL} \\ V_{qc} \\ V_{dc} \end{bmatrix} + \begin{bmatrix} \frac{1}{X_L}\omega_b & 0 \\ 0 & \frac{1}{X_L}\omega_b \\ 0 & 0 \\ 0 & 0 \end{bmatrix} \begin{bmatrix} V_{qs} - E_{qB} \\ V_{ds} - E_{dB} \end{bmatrix} \quad (14)$$

Where V_{qc} and V_{dc} are the series capacitor voltages and currents. V_{qs} , V_{ds} , E_{qB} , and E_{dB} are the stator and infinite bus

voltages. All of these parameters are shown in the qd0-frame.

3. SSR and Methods of its Analysis

Now, the consent of SSR is examined. Eigenvalue is explained as the method of analysis for a linear systems. Finally, intelligent methods are reviewed for fuzzy logic.

3.1. Definition of SSR

The SSR phenomenon is the state in which the wind plant exchanges in one or more natural frequencies with the electrical grid. This phenomenon can cause damages when it is not prevented. The SSR phenomenon is related to inductive generating and torsional interference effects. In a network with capacitive series compensation, the network has a natural frequency which is calculated by Equation (15), where fn is the resonant frequency called sub-synchronous, and its unit is Hertz. fs shows that synchronous frequency and Xl are the total reactance of the inductor, transformers, and inductor (Figure 1). Xc indicates the reactance of a series capacitor, which is the percentage of the reactance, and Xl is called the compensation percentage (% K). Due to frequency fn, slip Sn is introduced according to Equations (16) (Tapia, 2003) (Mohammadpour H. A., Sub-synchronous resonance analysis in DFIG-based wind farms: Definitions and problem identification—Part I., 2014, September).

$$fn = fs\sqrt{\frac{Xc}{Xl}} \tag{15}$$

$$Sn = \frac{fn-fr}{fn} \tag{16}$$

Since Sn is usually negative, the equivalent resistance of the rotor at the sub-synchronous frequency (Req/Sn) is negative. In other words, fr is negative when the amplitude of this resistor is more than the sum of the network and armature resistors.

Since S_n is negative, the equivalent resistance of the rotor at the subsynchronous frequency ($\frac{R_{eq}}{S_n}$) is negative. In other words, f_r is negative when the amplitude of this resistor is more than the sum of the network and armature resistors. As shown in the second part of Eq. (17), the current of the whole system will have an exponential function with positive power. Subsynchronous component with frequency of f_n appears in the currents, and voltages of the stator and mains circuit with the existence of capacitive series compensator. The complementary frequency of this component appears as IGE in the rotor current (15 Fateh, 2020). If the frequency, the torsional mode between the two masses of the rotor shaft with a complementary frequency of the network ($f_n - f_r$) is equal to or close to it. The torsional interaction (TI) effect occurs when the frequency of the torsional mode between the two masses of the rotor shaft with a complementary frequency of the network ($f_n - f_r$) is equal or close to each other. The frequency of the torsional modes of their rotors is low due to the low stiffness of the rotor shafts of wind farms. Thus, SSR occurs in wind power due to the effect of torsional interaction (TI). Thus, there is a need for a very high level of compensation (Liu, 2016). In addition, the probability of its occurrence is very low since it requires very high compensation (Mohammadpour H. A., Sub-synchronous resonance analysis in DFIG-based wind farms: Definitions and problem identification—Part I., 2014, September).

$$i(t) = \mathrm{A}\sin(2\pi f_s \mathrm{t}) + e^{\frac{R_{eq}}{L}t} B\sin(2\pi f_n \mathrm{t} + \partial) \tag{17}$$

3.2. *Eigenvalue of system*

The general state space of the network is modeled around its equilibrium point, depending on wind speed and level of compensation of the capacitor of series using the Linmod command obtained in MATLAB software. In this regard, 20 eigenvalues are obtained from the general state space of the network (Liu, 2016), among which four eigenvalues for induction machine, three for shaft system, eight for RSC and GSR of DFIG, four for transmission line with series capacitor, and one for dc link which form the 20th degree model. Table 2 indicates the system eigenvalues for compensation level of 70% and wind speed of 8m/s. As shown, the real values of all modes are negative except for the $\lambda 1$, $\lambda 2$modes, which represents the sub-synchronous mode for the instability of this mode.

Table 2
Eigenvalues for compensation level 75% and wind speed 7m/s

Mode	Eigenvalues	Mode	Eigenvalues
$\lambda 1$	+0.273+j123.26	$\lambda 11$	-0.023+j30.56
$\lambda 2$	+0.273-j123.26	$\lambda 12$	-0.023-j30.56
$\lambda 3$	-6.152+j628.42	$\lambda 13$	-109.60
$\lambda 4$	-6.152-j628.42	$\lambda 14$	-568.235
$\lambda 5$	-9. 412+j95.78	$\lambda 15$	-89.65
$\lambda 6$	-9. 412-j95.78	$\lambda 16$	-0.45
$\lambda 7$	-1.150+j4.260	$\lambda 17$	-0.254
$\lambda 8$	-1.150-j4.260	$\lambda 18$	-22.02
$\lambda 9$	-189.210-j1245.45	$\lambda 19$	-14.25
$\lambda 10$	-189.210+j1245.45	$\lambda 20$	-0.003

3.3. Review of fuzzy system

Fuzzy logic is considered as a method for reasoning which is similar to the way humans make reason. The fuzzy logic approach mimics the human decision-making method, in which all possible intermediate states between the digital values of "yes" and "no" are considered. Fuzzy logic has four main parts, as discussed below (Momoh, 1995).

Rule base: This section includes all of the rules and conditions which are specified as "if-then" by an expert to be able to control the decisions of a "decision-making system". Based on the new methods in fuzzy theory, it is possible to adjust and reduce the rules and regulations so that the best results can be obtained with the least rules.

Fuzzifire: In the fuzzy step, the inputs are converted to fuzzy

information. In other words, the numbers and information to be processed will become fuzzy sets and numbers. Input data are measured, for example, by sensors in a control system, which are modified and prepared for fuzzy logic processing.
Inference engine: In this section, the degree of compliance of fuzzy input with the basic rules is determined. In this way, different decisions are generated as a result of the fuzzy inference engine based on the percentage of compliance.
Defuzzifire: In the last step, the results of fuzzy inference, which are fuzzy sets, are converted into quantitative data. At this stage, you choose the best decision according to the outputs, which include different decisions with different percentages of compliance. This choice is normally based on the maximum degree of compliance. Fig. 5 shows all of the above-mentioned parts (Tomsovic, 1993):

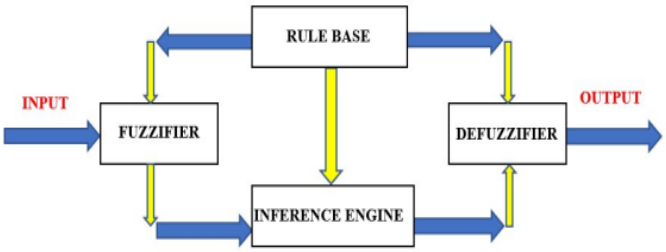

Fig. 5. Model of fuzzy system

4. Modelling of Wide Area Fuzzy Controller in the System Under Study

4.1. Review of wide area measurement systems

By combining the capabilities of telecommunication systems and digital measuring devices and controllers, WAMS enables the monitoring, protection, and control of the smart grid over a wide area. In general, WAMS consists of three subsystems including measurement, telecommunication, and processing. The system consists of several PMUs and one or more PDCs connected by a high-speed telecommunications network, as shown in Figure. 6 (Momoh, 1995).

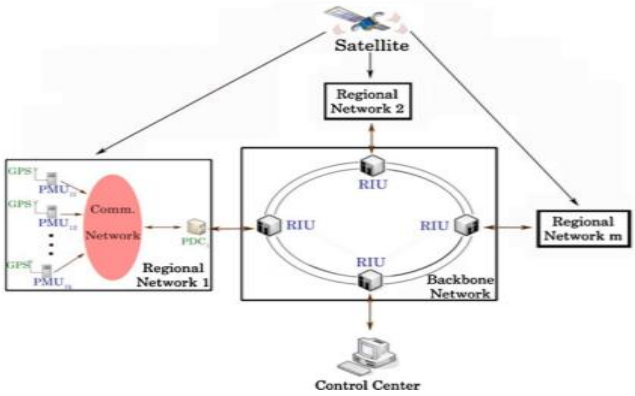

Fig. 6. Hierarchical structure of a WAMS.

4.2. fuzzy controller based on wide area measurement system

In the hierarchical structure of the WAMS proposed in (Momoh, 1995), the communication network is an optic fiber mesh net based on the wavelength division multiplexing (WDM) technology. As can be seen in Fig. 6, the WAMS is divided into several regional networks. Each region consists of a number of system buses and their emanated transmission lines. As it can be understood from this hierarchical structure, the geographical position of the system buses is a significant factor that should be considered in the power system partitioning. Therefore, it is imperative that the system buses in a regional network are geographically close to each other. This accordingly decreases the data transmission delay and increases the reliability of the communication network. The required data by the operator for various operational decisions, such as restorative actions, is another factor in the power system partitioning.
This section is to demonstrate the ability of FLC in damping SSR using WAMS signals. The IEEE Modified first benchmark test system, shown in Fig. 1, is utilized as the study testbed and its parameters are specified in (Piwko, 2006). In this study, in order to attenuate the fluctuations caused by SSR, a wide area fuzzy controller called the FLWADC controller has been used. This controller is applied to the output voltage control section of the stator of the terminal voltage generator (GSC converter controller).

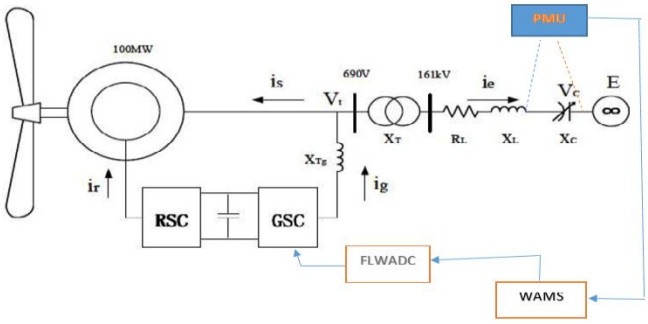

Fig. 7. Location of Fuzzy logic based on wade area in studed model

Figure 7 shows the location of the fuzzy controller, which is applied to the input of the stator voltage control loop of GSC.

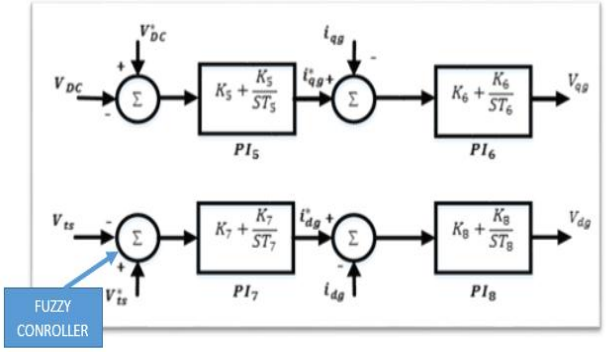

Fig. 8. Location of Fuzzy logic System

The fuzzy controller is based on the Mamdani inference model. Fuzzifier, Defuzzifier, inference methods, and fuzzy rules are the main parts of the controller. The input of the fuzzy system consists of two capacitor voltage signals of the compensator and the current passing through the capacitor, which is the same as the capacitor derivative, apply. In fact, a fuzzy model of a system is designed based on complete prior knowledge of that system.

The developed FLWADC is designed based on the Mamdani inference engine (Tomsovic, 1993). The fuzzification process, defuzzification, rule base, and inference engine are essential parts of fuzzy controller which are clarified in the following.

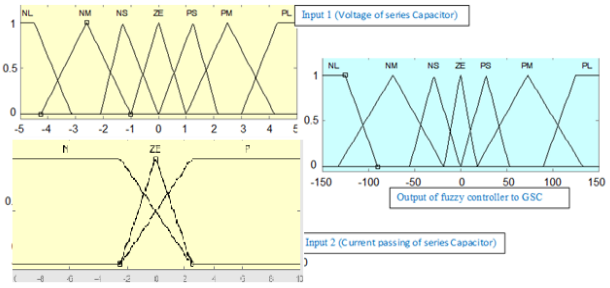

Fig. 9. Inputs and output membership functions

4.2.1. Fuzzification

Fuzzy controller input is the capacitive compensating voltage (V_c) of the transmission line series and its changes ($\frac{dV_c}{dT}$), the membership function of which is considered as follows based on the fuzzy rules. Fig. 9 displays the capacitor voltage with seven membership function and its changes with three membership function, as well as fuzzy controller output with seven membership function, which is considered as the knowledge of an expert. As shown, the symbols are defined as negative large (NL), negative (NM), medium, negative small (NS), zero (ZE), positive small (PS), positive medium (PM), positive large (PL), negative (N), and positive (P).

4.2.2. Rule base and inference engine

As mentioned, the fuzzy rules are based on Mamdani type, in the form of if …then, and in the form of 21 fuzzy relations according to the inputs and outputs of the fuzzy system, as shown in Table 3. For instance, as shown in Table 3, if V_c is NS, and $\frac{dV_c}{dT}$ is N, then the output is NM.

Table 3
Fuzzy rules based on fuzzy system inputs and output

V_c \ $\frac{dV_c}{dT}$	P		ZE
PL	PL	PL	PL
PM	PL	PS	PM
PS	PM	ZE	PS
ZE	PM	NM	ZE
NS	ZE	NM	NS
NM	NS	NL	NM
NL	NM	NL	NL

4.2.3. Defuzzification

Finally, the output of the fuzzy system should be converted to a crisp number. In this study, the average center of gravity was used.

5. Results of Time Domain Simulation

IEEE first benchmark modified DFIG based wind farm system was used to evaluate the proposed controller, and MATLAB/Simulink software was applied for simulating the time of the studied system. As mentioned before, the percentage of compensation of the transmission line is considered as one of the influential factors in SSR fluctuations, which increases with the percentage of compensation of the system towards instability. The modes of the studied system were expressed by using the eigenvalues method in Table 2, indicating that λ1 and λ2 are the oscillation modes of the system in the case where the compensation percentage is 25, 40, 60, and 75, as represented in Table 4. In this oscillating mode, the resonance frequency is 37.56 Hz, and the SSR frequency is 22.44 Hz. The contents of Eq. (18) indicated an increase in the percentage of compensation causes for the resistance of the whole system for being negative leading to instability in the system.

$$K\% \rightarrow X_c \rightarrow f_n = f_s\sqrt{\frac{X_c}{X}} \rightarrow s_n = \frac{f_n - f_r}{f_n} \rightarrow R_{eq} \leq 0$$
$$R_{eq-r} = \frac{R_r}{s_n} \rightarrow \quad (18)$$

Table 4
SSR mode and eigenvalues for compensation levels with wind speed 7m/s

Resonance Frequency	**SSR Frequency**	**SSR Mode ($\lambda 1, 2$ $Table(1)$)**	**Level of compensation (%)**
37.56	22.44	+11.650+j130.21	75
35.74	24.26	+5.760+j148.35	60
30.46	29.54	-1.25+j185.54	40
22.8	37.2	-4.66+j231.20	25

Figure. 10 shows the compensation system in the case where the compensation percentage is 25 and the system is stable. In the third of the simulation, the compensation percentage increases to 75, and the parameters are unstable.

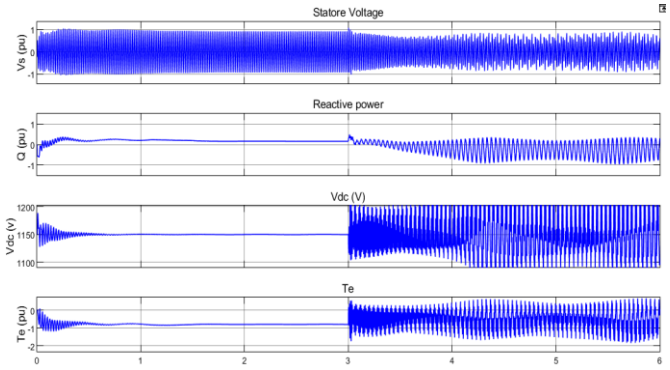

Fig. 10 capacitor voltage, reactive power stator voltage and electrical torque in k=25% to k= 75%&v=7m/s without damping

5.1. *fuzzy controller based on wide area measurement system*

This part of the simulation shows the application of fuzzy controllers to the studied system in the case where the delays caused by the measured PMU signals are ignored. As shown in Figure 7, SSR fluctuations are damped by applying a controller to the stator voltage control loop in the GSC. The membership functions of Fig. 5 are quenched by the SSR fluctuations with the 21 fuzzy rules in Table 3 and receiving the controller inputs, which is the same as the capacitor compensating voltage and its changes from the PMU, as shown in Figure. 11.

As displayed in Fig. 11, the oscillations are damped in the case where the compensation percentage is 75 and the system is unstable in the third second of the simulation by applying a fuzzy controller.

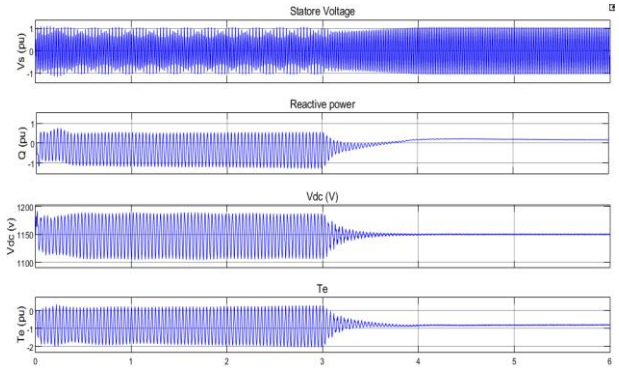

Fig. 11. Damping of capacitor voltage, reactive power and stator and electrical torque in k=75%& v=7m/s with fuzzy controller

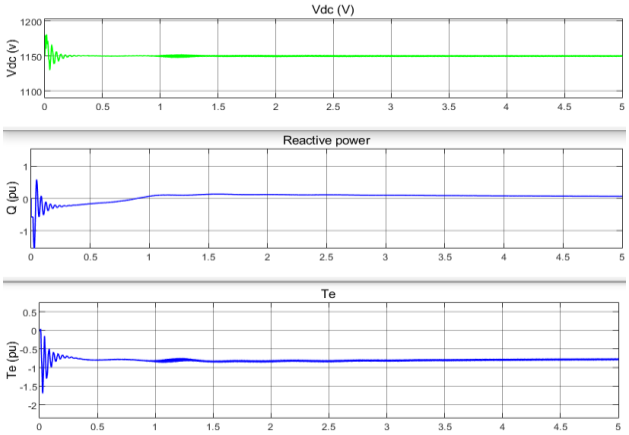

Fig. 12. Damping of capacitor voltage, reactive power and stator and electrical torque in k=80%& v=7m/s with fuzzy controller

Figures. 12 and 13, show capacitor voltage, reactive power, and stator, and electrical torque in k=80%& 85 with the fuzzy controller. When the FLWADC with time delay is in service, the system is stable.

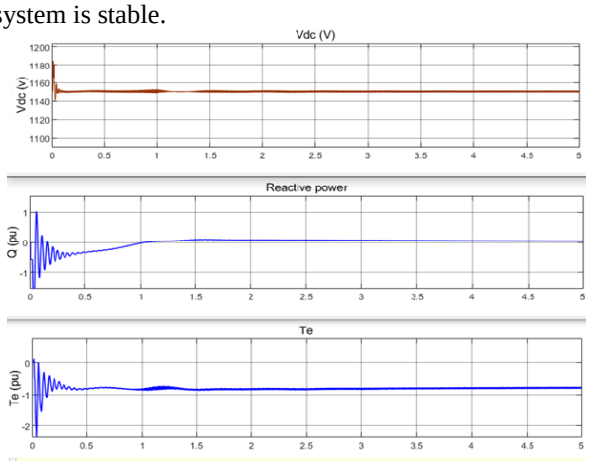

Fig. 13. Damping of capacitorvoltage, reactive power and stator and electrical torque in k=85%& v=7m/s with fuzzy controller

5.2. *Comparison with previous research*

To compare the proposed method in this paper, the results are compared with the methods that have been worked on before. As mentioned in the various references, considering the control structure of figure 16, it is possible to optimize its parameters by optimizing the objective function 19 with the PSO and ICA optimization methods.

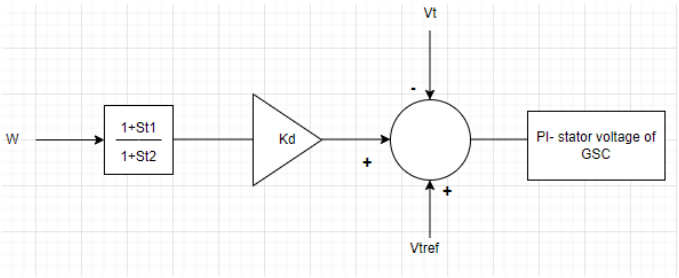

Fig. 14. strauctureod damping controller with optimazation methods

$$Objective\ Function = min(f)$$
$$f = \int_{t=0}^{t=t_{sim}} t|\Delta\omega|dt \quad (19)$$

In Eq. 19, t_{sim} represents the simulation time, Δω the deviations of the induction generator's speed. To calculate the objective function, the time domain of the system model must be simulated with respect to all saturation constraints. The permissible limit k_d is between zero, and one.

Table 5 shows the results of optimization of Objective function (19) by both PSO and ICA methods.

Table 5
The value of Coefficient k_d

Methods of optimization	k_d
PSO	0.64
ICA	0.72

In addition, Figures 15 and 16 show the speed deviation of generators with PSO and ICA algorithms.

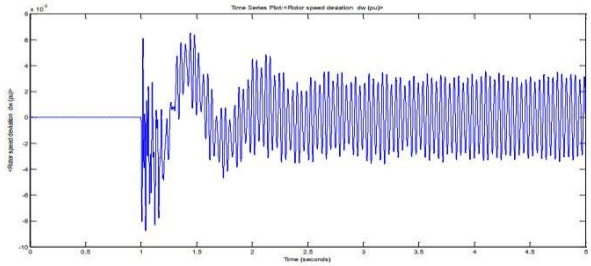

(a)

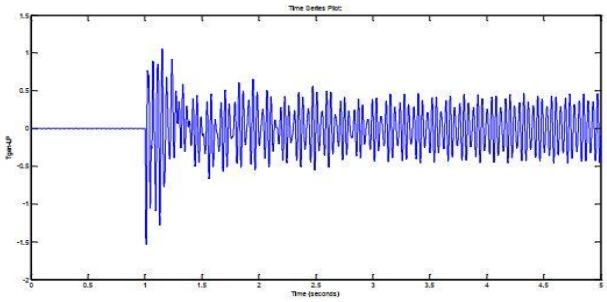

(b)

Fig. 15. Damping of SSR with ICA method

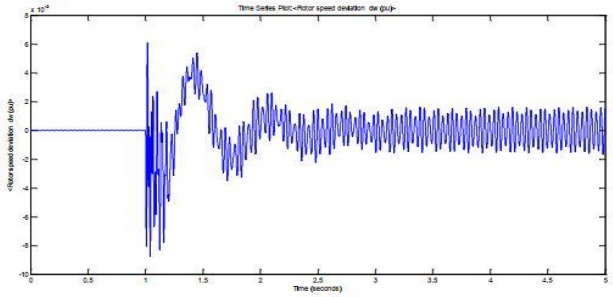

(a)

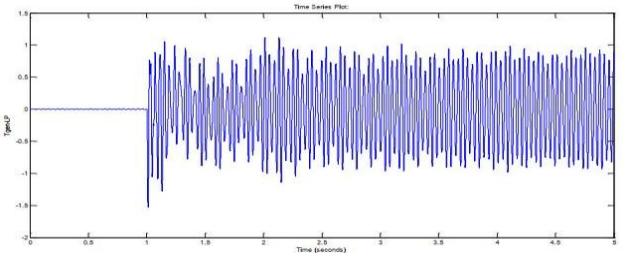

(b)

Fig. 16. Damping of SSR with PSO method

In addition, a comparison of Figures 15 and 16 with Figures 11,12, and 13, shows that the proposed WAMS-based fuzzy controller method is faster. Another important point in the proposed method in this paper is no adjustment of parameters at each level compensates for transmission lines.

6. Conclusion

In this study, a new method was used for damping SSR fluctuations of a DFIG-based wind farm with the fuzzy controller and using WAMS in power systems. No need to adjust the parameters of the controller, as well as work at a high level of compensation, namely 75%, and using WAMS is the main feature of this controller. In addition, the results of the proposed method as compared with the methods that have been worked based on optimization metaheuristic PSO, ICA. The effectiveness of this controller in damping SSR fluctuations has been demonstrated by time simulation using Matlab/Simulink software on a modified version of the IEEE first benchmark model with DFIG.

Table 6
Parameter of DFIG-based wind farms

Base Power	2 MW	100 MW
Based voltage (VLL)	690 V	690 V
Xls	0.09231	0.09231
Xlr	0.09955	0.09955
Rs	0.00488	0.00488
XM	3.95279	3.95279
Xtg	0.3 (0.189 mH)	0.3 (0.189/50 mH)
DC-link base voltage	1200 V	1200 V
DC-link capacitor	14000 µF	50*14000 µF

References

Li, Y., Xie, X., Liu, H., Liu, H., , & Zhang, C. (2017). Mitigation of sub-synchronous control interaction in wind power systems with GA-SA tuned damping controller. IFAC-PapersOnLine, 50(1), 8740-8745.

Mohammadpour, H. A., & Santi, E. (2015). Optimal adaptive sub-synchronous resonance damping controller for a series-compensated doubly-fed induction generator-based wind farm. IET Renewable Power *Generation*, *9*(6), 669-681.

Mohammadpour, H. A., & Santi, E. (2015). Optimal adaptive sub-synchronous resonance damping controller for a series-compensated doubly-fed induction generator-based wind farm. *IET Renewable Power Generation*, *9*(6), 669-681.

Miller, N. W., Sanchez-Gasca, J. J., Price, W. W., & Delmerico, R. W. (2003, July). Dynamic modeling of GE 1.5 and 3.6 MW wind turbine-generators for stability simulations. In *2003 IEEE Power Engineering Society General Meeting (IEEE Cat. No. 03CH37491)* (Vol. 3, pp. 1977-1983). IEEE.

Mohammadpour, H. A., & Santi, E. (2014). Modeling and control of gate-controlled series capacitor interfaced with a DFIG-based wind farm. *IEEE Transactions on Industrial Electronics*, *62*(2), 1022-1033.

Mohammadpour, H. A., & Santi, E. (2015). Optimal adaptive sub-synchronous resonance damping controller for a series-compensated doubly-fed induction generator-based wind farm. *IET Renewable Power Generation*, *9*(6), 669-681.

Mohammadpour, H. A., & Santi, E. (2014, September). Sub-synchronous resonance analysis in DFIG-based wind farms: Definitions and problem identification—Part I. In *2014 IEEE Energy Conversion Congress and Exposition (ECCE)* (pp. 812-819). IEEE.

Mohammadpour, H. A., Shin, Y. J., & Santi, E. (2014, March). SSR analysis of a DFIG-based wind farm interfaced with a gate-controlled series capacitor. In *2014 IEEE Applied Power Electronics Conference and Exposition-APEC 2014* (pp. 3110-3117). IEEE.

Mohammadpour, H., & Santi, E. (2015). SSR damping in wind farms using observed-state feedback control of DFIG converters. *Electric Power Systems Research*, *123*, 57-66.

Moharana, A., Varma, R. K., & Seethapathy, R. (2014). SSR alleviation by STATCOM in induction-generator-based wind farm connected to series compensated line. *IEEE Transactions on Sustainable Energy*, *5*(3), 947-957.

Momoh, J. A., Ma, X. W., & Tomsovic, K. (1995). Overview and literature survey of fuzzy set theory in power systems. *IEEE Transactions on power systems*, *10*(3), 1676-1690.

Naduvathuparambil, B., Valenti, M. C., & Feliachi, A. (2002, March). Communication delays in wide area measurement systems. In *Proceedings of the thirty-fourth southeastern symposium on system theory (Cat. No. 02EX540)* (pp. 118-122). IEEE.

Piwko, R., Miller, N., Sanchez-Gasca, J., Yuan, X., Dai, R., & Lyons, J. (2006, August). Integrating large wind farms into weak power grids with long transmission lines. In 2006 CES/IEEE 5th International Power Electronics and Motion Control Conference (Vol. 2, pp. 1-7). IEEE.

Raiesdana, S. (2021). A Hybrid Method for Industrial Robot Navigation. *Journal of Optimization in Industrial Engineering*, *14*(1), 219-234.

Rajaram, T., Reddy, J. M., & Xu, Y. (2016). Kalman filter based detection and mitigation of subsynchronous resonance with SSSC. *IEEE Transactions on Power Systems*, *32*(2), 1400-1409.

Raju, D. K., Umre, B. S., Junghare, A. S., & Babu, B. C. (2016). Improved control strategy for subsynchronous resonance mitigation with fractional-order pi controller. *International Journal of Emerging Electric Power Systems*, *17*(6), 683-692.

Raju, D. K., Umre, B. S., Junghare, A. S., & Babu, B. C. (2017). Mitigation of subsynchronous resonance with fractional-order PI based UPFC controller. *Mechanical Systems and Signal Processing*, *85*, 698-715.

Rohit, C., Darji, P., & Jariwala, H. (2021). Modeling and Control of Static Synchronous Series Compensator Interfaced with DFIG-Based Wind Farm using PSO for SSR Alleviation. *International Journal of Ambient Energy*, (just-accepted), 1-24.

Sahni, M., Badrzadeh, B., Muthumuni, D., Cheng, Y., Yin, H., Huang, S. H., & Zhou, Y. (2012, July). Sub-synchronous interaction in Wind Power Plants-part II: An ercot case study. In *2012 IEEE Power and Energy Society General Meeting* (pp. 1-9). IEEE.

Suriyaarachchi, D. H. R., Annakkage, U. D., Karawita, C., Kell, D., Mendis, R., & Chopra, R. (2012, July). Application of an SVC to damp sub-synchronous interaction between wind farms and series compensated transmission lines. In *2012 IEEE Power and Energy Society General Meeting* (pp. 1-6). IEEE.

Tapia, A., Tapia, G., Ostolaza, J. X., & Saenz, J. R. (2003). Modeling and control of a wind turbine driven doubly fed induction generator. *IEEE Transactions on energy conversion*, *18*(2), 194-204.

Tomsovic, K., Tapper, M., & Ingvarsson, T. (1993). A fuzzy information approach to integrating different transformer diagnostic methods. *IEEE Transactions on Power Delivery*, *8*(3), 1638-1646.

Vajpayee, S., Panda, N. R., Behera, P., & Swain, S. C. (2020, July). Implementation of PLL algorithm in DFIG based wind turbine connected to utility grid. In *2020 Second International Conference on Inventive Research in Computing Applications (ICIRCA)* (pp. 549-553). IEEE.

Wang, Y., Wu, Q., Yang, R., Tao, G., & Liu, Z. (2018). H∞ current damping control of DFIG based wind farm for

sub-synchronous control interaction mitigation. *International Journal of Electrical Power & Energy Systems*, *98*, 509-519.

Wang, L., Xie, X., Jiang, Q., & Pota, H. R. (2013). Mitigation of multimodal subsynchronous resonance via controlled injection of supersynchronous and subsynchronous currents. *IEEE Transactions on Power Systems*, *29*(3), 1335-1344.

Xu, L., & Cartwright, P. (2006). Direct active and reactive power control of DFIG for wind energy generation. IEEE Transactions on energy conversion, 21(3), 750-758.

Xie, H., & de Oliveira, M. M. (2014, October). Mitigation of SSR in presence of wind power and series compensation by SVC. In 2014 International Conference on Power System Technology (pp. 2819-2826). IEEE.

Xu, L., & Wang, Y. (2007). Dynamic modeling and control of DFIG-based wind turbines under unbalanced network conditions. IEEE Transactions on power systems, 22(1), 314-323.

Xie, H., Li, B., Heyman, C., De Oliveira, M. M., & Monge, M. (2014). Subsynchronous resonance characteristics in presence of doubly-fed induction generator and series compensation and mitigation of subsynchronous resonance by proper control of series capacitor. IET renewable power generation, 8(4), 411-421.

Zhang, X., Xie, X., Liu, H., Liu, H., Li, Y., & Zhang, C. (2017). Mitigation of sub-synchronous control interaction in wind power systems with GA-SA tuned damping controller. IFAC-PapersOnLine, 50(1), 8740-8745.

This article can be cited: Bostani, Y., & jalilzadeh, S. (2022). A New Fuzzy Controller for Damping of Sub Synchronous Resonance (SSR) in the Modified IEEE First Bench Mark. *Journal of Optimization in Industrial Engineering*, *15*(2), 45-55.
Doi: 10.22094/joie.2022.1943281.190